



The Abdus Salam
International Centre for Theoretical Physics



EMAS 2008

8th EMAS Regional Workshop on
**Electron Probe Microanalysis
of Materials Today**
Practical Aspects
including a session on
synchrotron-based microanalysis

19 - 22 April 2008
Adriatico Guesthouse
The Abdus Salam International Centre for Theoretical Physics
Trieste, Italy

Book of Abstracts

MICRO-X-RAY ABSORPTION SPECTROSCOPY (XANES, EXAFS)

Francesco d'Acapito*

CNR-INFM - OGG c/o European Synchrotron Radiation Facility -
GILDA CRG
P.O. Box 220, FR-38043 Grenoble, France
* dacapito@esrf.fr



INTRODUCTION TO X-RAY ABSORPTION SPECTROSCOPY (XAS)

X-ray absorption spectroscopy (XAS) is an experimental technique that provides information on the electronic and atomic structure in the vicinity of a chosen element. This is done by analysing the features that appear in the X-ray absorption coefficient, μ , of a core state (usually K or L): peaks on the absorption edge and up to $\cong 50$ eV above (called XANES region, X-ray Absorption Near Edge Structures) or oscillations (called EXAFS region, Extended X-ray Absorption Fine Structure) extending up to around 0.5 - 2 keV above. These oscillations appear only when the absorbing atom is surrounded by other atoms (they do not appear in the spectra of noble gases in the gaseous state) and examples of spectra are shown in Fig. 1.

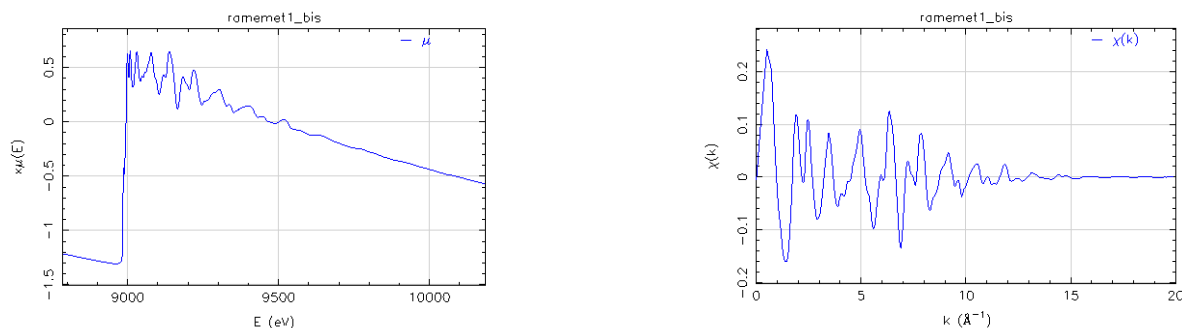


Fig. 1. Left: an example of EXAFS oscillations in the X-ray absorption coefficient, μ , of metallic Cu at the Cu K edge ($E = 8,979$ eV).
Left : the whole χ as a function of the photon energy E ;
Right: the EXAFS oscillations isolated from the background.
The spectra were collected at the GILDA CRG Beamline at European Synchrotron Radiation Facility (ESRF) [1].

On the left side of Fig. 1 is shown the absorption coefficient, μ , of metallic Cu at the Cu-K edge region. The oscillations extending up to 600 eV above the edge constitute the EXAFS signal. On the right side, the oscillations, after removal of the atomic background, are shown. The first observation of the phenomenon were made in the early '30s but only recently,

with the use of Fourier Transform technique for data analysis [2] and the advent of the synchrotron radiation sources [3], the technique has received great attention. A general review on the technique is given in [4, 5], whereas a recent review on the theoretical aspects linked to EXAFS is presented in [6].

Extended X-ray absorption fine structure (EXAFS)

The physical origin of the μ -oscillations above the edge is the modification, due to the neighbouring atoms, of the final state of the electron emitted by the atom that absorbs the incoming X-ray photon (hereafter called "Central" or "Absorber" atom). The X-ray absorption cross-section, σ , of an atom interacting with a photon described by a dipole transition operator \vec{D} is given by [7]:

$$\sigma = 4\pi^2 E \alpha \sum_f \left| \langle i | \vec{p} \cdot \vec{D} | f \rangle \right|^2 \delta(E - E_f + E_0) \quad (1)$$

where E is the photon energy, α the fine structure constant, E_f is the photoelectron energy and E_0 is the threshold energy. $\langle i |$ and $\langle f |$ are, respectively, the initial and final electron states, and \vec{p} is the electron momentum operator. The initial state $\langle i |$ is usually an atomic core state (K or L) so it is strongly localized around the central atom site: this means that σ has to be calculated in a restricted region around the absorber. In the case of the isolated atom $\langle f |$ is an outgoing spherical wave where k is the photoelectron wavevector

$$k = \sqrt{2m(E - E_0)}/\hbar$$

In this case, $\langle f |$ is a smooth and structureless function of E , so the absorption cross-section σ_0 for an isolated atom will not contain oscillations.

When a neighbour (backscattering atom) is added to the central atom, a part of the outgoing electron wave will be backscattered by the neighbour as shown in Fig. 2.

$\langle f |$ will be the sum of the original outgoing wave plus a modified part, coming from the waves backscattered by the neighbours. The backscattered wave will have an amplitude $A(k, R_j)$ and a phase $\varphi(k, R_j)$ both depending on the details of the scattering potential. The interference between the initial and final state in the absorber site gives rise to the oscillations observed in the experimental data.

The oscillatory part χ of the signal is defined considering σ_0 and the total cross-section σ taking:

$$\chi \equiv \frac{\sigma - \sigma_0}{\sigma_0}$$

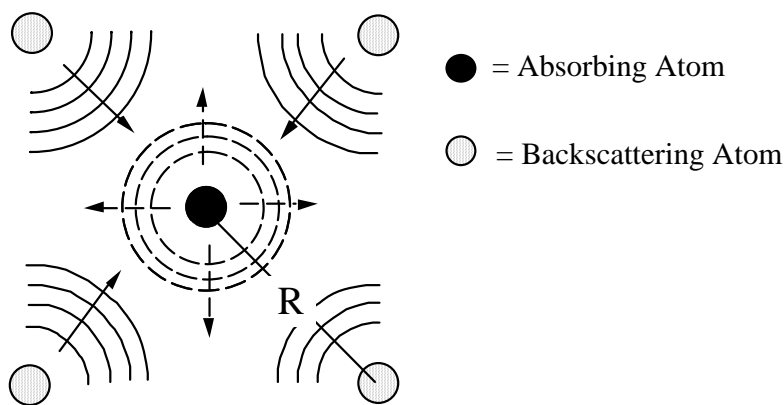


Fig. 2. A pictorial view of the EXAFS effect: the outgoing electron wave (dashed line) is partially scattered backward by the neighbouring atoms. This causes a modification of the final state that is responsible for the oscillations in the absorption coefficient.

The explicit expression for χ in the case of a 'S' state excitation and considering only single scattering events is [4]:

$$\chi = \sum_j \chi_j = \sum_j 3S_0^2 \frac{N_j}{kR_j^2} A(k, R_j) \sin[2kR_j + \varphi(k, R_j) + 2\delta_c(k)] e^{-k^2\sigma_j^2} e^{-2R_j/\lambda} (\hat{e} \cdot \hat{R}_j)^2 \quad (2)$$

Here the sum is extended over the various coordination shells indexed by j , each containing N_j identical atoms at a distance R_j from the central one. The backscattering amplitude $A(k, R_j)$ and phase, and $\varphi(k, R_j)$, are expressed in terms of the bond length R_j (curved wave approximation). In Eq. (2) \hat{e} is the field polarisation unit vector and the related term expresses the dependence of χ on the beam polarisation. This dependence comes from the $\mathbf{p} \cdot \mathbf{D}$ operator and is of particular interest for single crystal samples, where the absorption coefficient depends on the sample orientation. Conversely, in the case of isotropic samples (polycrystalline powders, amorphous samples, liquids, ...), the $(\hat{e} \cdot \hat{R}_j)^2$ term is replaced by its angular average, 1/3.

In the $\chi(k)$ formula shown above other terms are added to the simple scattering approximation in order to account for additional processes affecting the amplitude of the oscillations. The first one is linked to the disorder in the atomic positions. This can be originated by thermal vibrations or by random positions of the neighbour atoms in amorphous systems. If we suppose a small disorder and a Gaussian pair distribution function with mean square displacement σ_j^2 , the result of the integral is the $\exp(-k^2\sigma_j^2)$ term in Eq. (2) [8]. If thermal disorder dominates, the values of σ_j can be calculated from the dynamic properties of the lattice under study, as shown in [8 - 10].

Another term is the limited lifetime of both the photoelectron and the core-hole. Indeed, the excited atom keeps this state for a limited time, after which an electron from the upper state fills the hole in the core state, destroying the EXAFS signal. Also, when the emitted

photoelectron undergoes momentum transfer or inelastic scattering with other electrons, the EXAFS signal is cancelled. This can be accounted for, by adding an imaginary part to the scattering potential [11] and is made explicit by the $\exp(-r_j/\lambda)$ term in Eq. (2). This is particularly important because, being λ of the order of a few Å, it limits the sensitivity of the technique to the very local atomic structure around the absorber. Simultaneously with the electron emission other electrons can also be excited in the central atom, both to bound states or continuum states [12]. This causes an overall reduction of the amplitude of the oscillations and it is accounted for by the S_0^2 term.

In the case of the EXAFS region a quantitative analysis of the data can be carried out, i.e. it is possible to obtain quantitative results for the local structure parameters: N (typ. error 10 %), R (typ. error 1 %) and σ^2 (typ. error 20 %). In practice, the Fourier transform of the $\chi(k)$ function is taken and then a back transform is carried out by filtering only the region around a given peak [4, 13]. The function obtained is then fitted to a formula like that in Eq. (2) with only a single term in the sum.

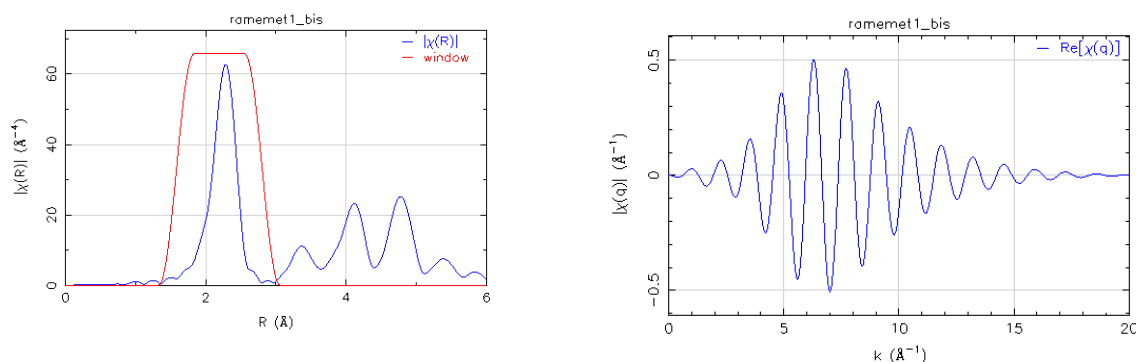


Fig. 3. Left: Fourier transform of the EXAFS oscillations shown in Fig. 1 right. The peaks correspond to the various coordination shells present in the crystalline face centred cubic structure of Cu. In particular the first shell (contoured by the back-transformation window in red) dominates the spectrum together with the second, third and fourth coordination shells. Right: the back Fourier transform of the previous spectrum containing only the oscillations due to the first coordination shell.

The present procedure can be easily adopted in cases where only a limited number of phases contribute to the total spectrum. To carry out a quantitative EXAFS analysis a number of programmes are available both for theoretical calculation of the backscattering parameters and for the structural fits to the experimental data [14 - 18].

When several phases, each consisting in a complex spectrum, are at the same time present in the spectrum a different approach is adopted. The EXAFS spectra can be either fitted to a linear combination of known compounds [19, 20] or, in a more sophisticated way, the so-called Principal Component Analysis (PCA) [21 - 23] is carried out. Following this

method, a set of spectra coming from the samples is reduced, by linear algebra methods, to a smaller set consisting in "basis" spectra. From the analysis of the basis spectra is then possible to retrieve the structural parameters of the original data.

X-ray absorption near edge structure (XANES)

In the vicinity of the absorption edge the energy of the photoelectron becomes lower so the associated wavelength well comparable with the atomic distances and the mean free path increases. In this region a simple treatment as that shown in Eq. (2) is no longer applicable and a more complex treatment is needed. The calculation of the absorption cross-section σ can be carried out in several ways, namely in the Green function approach where σ is expressed in matrix form [24]:

$$\sigma = \sigma_0 \left[\frac{1}{(2L_0 + 1) \sin^2 \delta_l^0} \sum_m \Im \left[(I - TG)^{-1} T \right]_{m,lm}^{0,0} \right] \quad (3)$$

Here, G is the so-called "Propagator matrix" and contains all the geometrical details of the cluster surrounding the absorber, and T is the "Scattering matrix" and it contains the details of the scattering potentials. This region of the spectrum is called XANES (X-ray Absorption Near Edge Structure) and it contains in principle 3-dimensional information on the absorber site (Fig. 4).

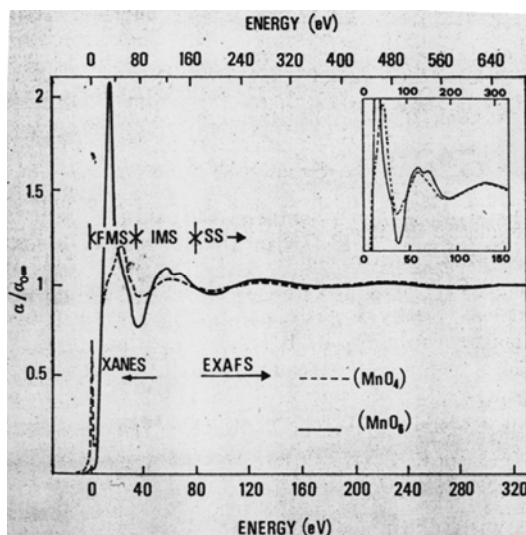


Fig. 4. Partition of a spectrum, in the EXAFS and XANES regions. Here the Mn-K edge spectra of tetrahedral $(\text{MnO}_4)^-$ and octahedral $[\text{Mn}(\text{H}_2\text{O})_6]^{2+}$ complexes in aqueous solution are shown [picture from 25]. Note the differences in the shape of the XANES region in the two cases: namely the peak at 0 eV that is present in the tetrahedral compound and absent in the octahedral one and the height of the white line. Both are related to the different symmetry of the complex.

Eq. 3 can be used to reproduce data in a quantitative way [26, 27] with a fitting routine that minimizes the differences between the experimental spectrum and the calculated one by varying the atomic spatial positions. As a matter of fact, this method revealed to be extremely powerful for clusters of limited dimensions as in metallo-proteins [27], but it represents a computationally extremely heavy task even in the case of clusters of some tens of atoms. In practice the XANES region is used for a more qualitative analysis based on the comparison with known compounds. In particular the edge position (i.e. the first inflection point of the absorption spectrum vs. energy) reveals the valence state of the chemical species in analysis; it falls at higher energies for increasing positive valence [28]. Moreover by the combined analysis of the position and intensity of peaks due to transitions to bound states (a typical case is the partially forbidden 1s-3d transition in transition metals) it is possible to infer the type of local symmetry (tetrahedral or octahedral) (see Fig. 4 and [29]). Finally, a more quantitative analysis can be carried out by reproducing the sample spectrum with linear combination of model spectra [20] or by PCA [23].

Synchrotron X-ray fluorescence (SXRF)

Finally, we will describe here the simpler case of data that can be collected with a microbeam that is the spatially resolved synchrotron X-ray fluorescence. The sample is scanned through the beam and at each point the intensity of the fluorescence line of a chosen chemical element is collected. In this way maps of the concentration (within the typical sampling depth values of X-rays i.e. a few tens of μm) of various elements can be derived and a comparison with optical microscope data can be carried out to state the relation between the element concentration and structures in the sample [30]. In order to obtain quantitative data on the correlation of, namely, two chemical species in a sample a cross correlation function $\rho(\delta)$ is defined as a function of the intensity $I(r)$ of the '1' and '2' species in a sample point r using averages ($\langle \rangle$) over the sample body as follows [20]:

$$\rho(\delta) = \frac{\langle (I_1(r) - \langle I_1 \rangle) * (I_2(r + \delta) - \langle I_2 \rangle) \rangle}{\sqrt{\langle (I_1(r) - \langle I_1 \rangle)^2 \rangle * \langle (I_2(r) - \langle I_2 \rangle)^2 \rangle}} \quad (4)$$

Alternatively, scatter plots presenting on the axes the counts of each of the two species on the same point [19] as shown in the picture below (Fig. 5).

DATA COLLECTION

X-ray optics

In order to analyze samples exhibiting spatial inhomogeneities it is mandatory to use a probe beam as small as possible. The size of the beam available on the sample critically depends on the source brilliance and on the capability of the focussing X-ray optical elements to preserve this parameter on the sample. The brilliance B of a source is defined as the number of photons per second emitted by a unit source area in a given solid angle and in a given energy

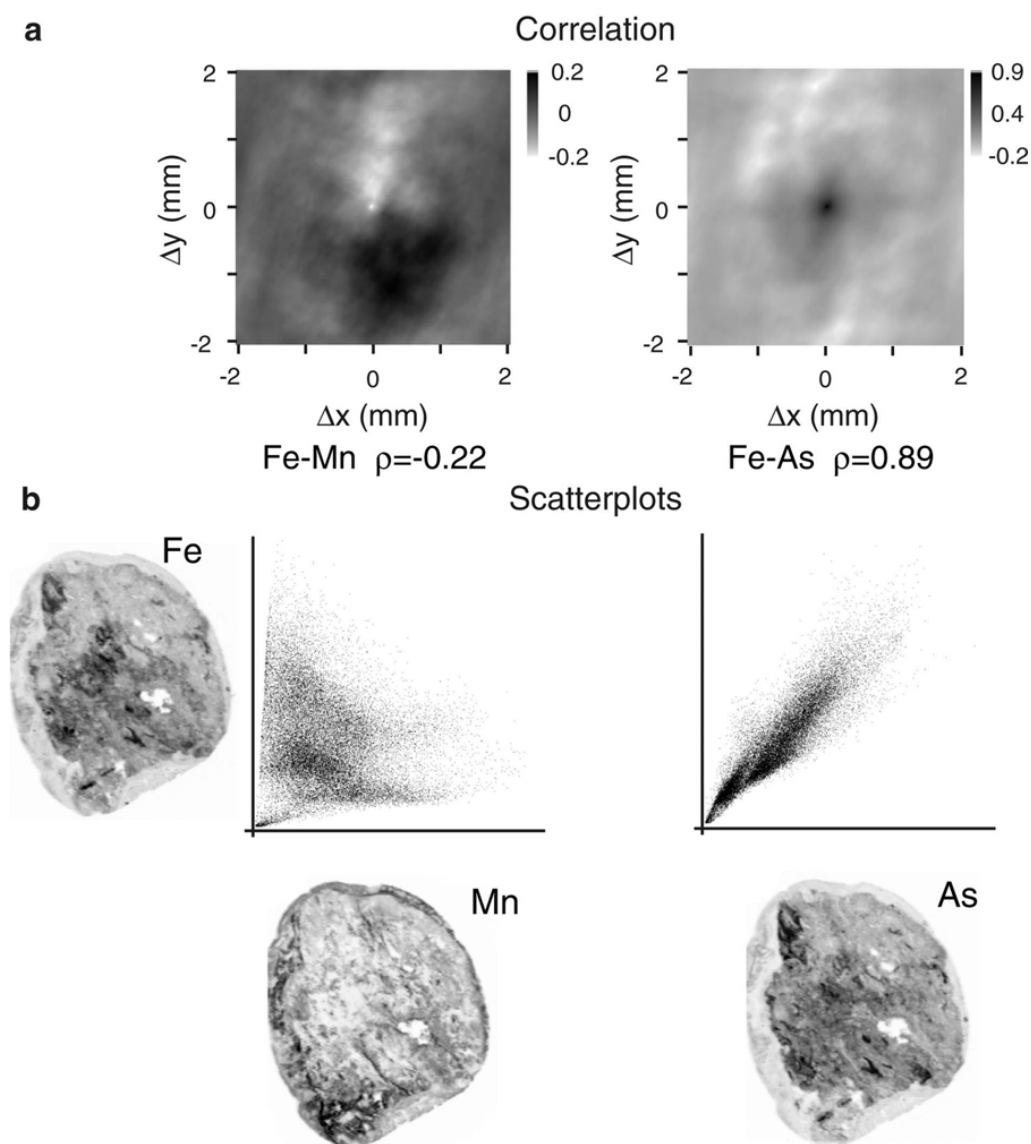


Fig. 5. Examples of cross correlation maps (a) and scatter plots (b) in the case of a soil nodule from the Morvan region (France) [19]. The data relative to Fe, As and Mn are presented. From the plots it is derived that Fe and Mn are slightly anti-correlated whereas Fe and As are strongly correlated. Picture from [19].

band: typical units used in synchrotron literature are $[B] = [\text{photons s}^{-1}\text{mm}^{-2}\text{mrad}^{-2} 0.1 \text{ \% bandwidth}]$. In recent years, with the advent of the so-called third generation synchrotron sources, experimental methods based on microbeams have received a noticeable improvement [31]. Indeed the brilliance of the source has increased from $B_2 \cong 10^{15} [\text{photons s}^{-1}\text{mm}^{-2}\text{mrad}^{-2} 0.1 \text{ \% bandwidth}]$ typical for the bending magnet sources in second generation machines to $B_3 \cong 10^{20} [\text{photons s}^{-1}\text{mm}^{-2}\text{mrad}^{-2} 0.1 \text{ \% bandwidth}]$ that is currently achieved on undulator sources. The availability of 'brilliant' sources has then allowed the realisation of microbeams by using suitable optics. A number of focussing elements are available in the X-ray region

such as zone plates [32], compound refractive lenses [33], capillaries [34], and mirrors [35]. In order to carry out efficient XAS experiments some requirements should be satisfied:

- i) the system should be achromatic in order to permit the collection of EXAFS spectra that typically span an energy region of about 10 % with respect to the edge value;
- ii) the system should permit sufficient space between the focal spot and the last optical element to permit the sample to be mounted on a motorized aligning stage, and/or different equipments like a cryo-cooler or an incoming beam monitor.

Not all focussing systems are suited for this purpose [31]: namely zone plates or refractive lenses are appreciably chromatic (so permitting only the collection of XANES data) whereas capillaries exhibit a too short focal length to satisfy point ii). The kind of focussing element best suited for this kind of investigations is the Kirkpatrick-Baez (KB) mirror assembly [35] that couples achromaticity with sufficient focal length. This device consists of two elliptical reflecting mirrors with orthogonal reflection planes and recently it has been demonstrated to be capable to provide focal spots in the 90 nm range [36].

As an example of a beamline for micro-XAS investigations we will present here the case of LUCIA formerly operated at the Swiss Light Source and soon operative at the SOLEIL synchrotron [37] (Fig. 6).

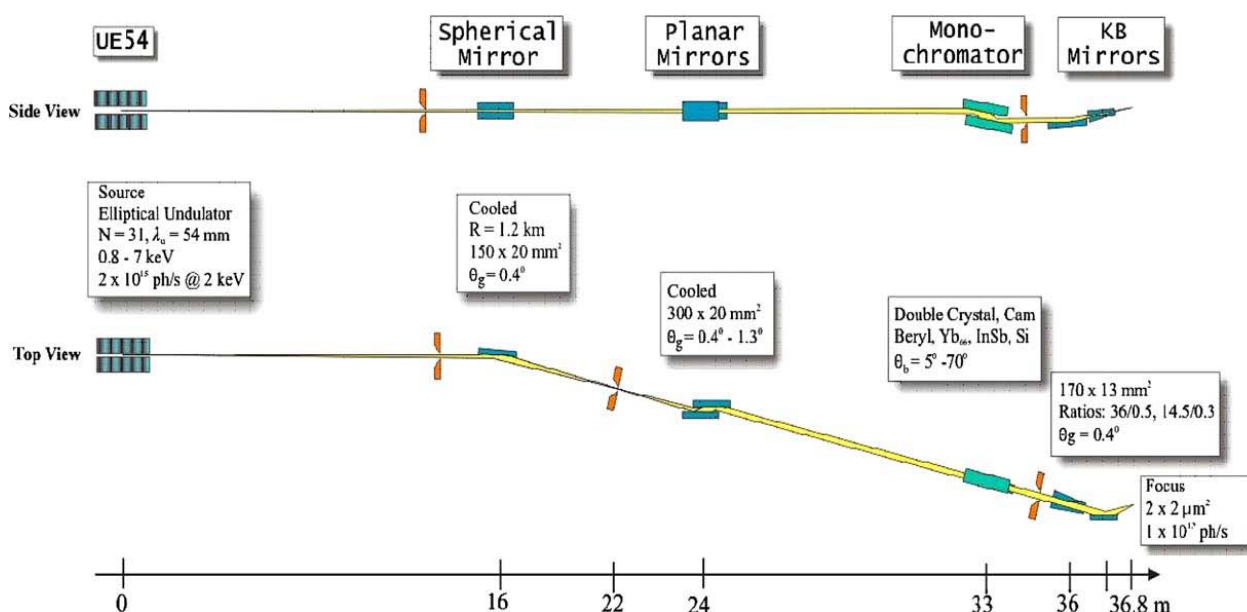


Fig. 6. Layout of the X-ray optical elements of the LUCIA beamline [picture from 37].

The source is an APPLE-II type undulator that provides linearly and circularly polarized light. By moving the jaws of the undulator it is possible to change the direction of the linear polarisation vector from horizontal to vertical thus permitting an easy analysis of non-cubic systems. At 16 m from the source a first spherical mirror focalizes the beam horizontally, creating a virtual source at 22 m. The double crystal (fixed exit) monochromator is placed at

24 m from the source behind the first mirror and the virtual source. Eventually, after the monochromator, the KB mirror assembly focusses the beam to a spot of about 2*2 μm . The beamline is operative in the energy range 0.8 - 8 keV and provides a photon flux $>10^{10}$ ph/s over the whole range. The sample is mounted on an x-y translation stage and a microscope is used for sample positioning. Similarly equipped beamlines are available on all the major high energy third generation synchrotron sources like ESRF (beamlines ID21 [38], and ID22 [39]), APS (2-ID-D, 18-ID-D, 13-ID-C,D, 20-ID-B,C, 10-ID-B [40]), and Spring-8 (BL37XU, BL39XU [41], BL47XU [42]).

Data collection

In general, the sample is scanned through the beam and different quantities can be measured at each sampling point:

- i) the intensity of the fluorescence of a given chemical species; in this case a map of concentration of this element is realized by scanning over the sample body;
- ii) a complete spectrum (XANES or EXAFS) can be collected thus also providing a map on the valence state or chemical environment.

The absorption coefficient, μ , of a sample as a function of the energy is defined as:

$$\mu(E) = -\ln \left[\frac{\Phi_1(E)}{\Phi_0(E)} \right] \quad (5)$$

where Φ_0 and Φ_1 are the photon fluxes before and after the sample respectively (Fig. 7, right). The fluxes Φ are measured by reading the current in ionisation chambers (called I_{c0} and I_{c1}), usually filled with low-pressure gas. However in the case of μ -XAS this would mean that the sample should be sliced at a thickness of a few microns in order to collect correctly the data but this condition is hardly achievable with common samples. More frequent is the case where the sample is analyzed without a preparation and the fluorescence detection mode is used [43] (Fig. 7, left).

Indeed, the photo-ionisation process creates a hole in the core state that is suddenly filled by another electron. This occurs through a couple of competitive processes: a radiative one, where an electron 'falls' from a higher energy state to the ionized one emitting a photon (fluorescence). Alternatively, hole filling can be accompanied by the emission of fast electrons to balance the energy (Auger processes). The higher the Z of the involved atom, the more probable is the fluorescence process, with equal probability occurring at roughly $Z = 30$. It must be noted that the emission of the fluorescence photon occurs at a well-determined energy, depending on the atom and on the level involved: it is thus easy to separate the desired signal from the background using an energy-resolving detector like Si(Li) or high-purity germanium [44]. In this case care should be devoted to avoid spectral distortions due to non-linear detector response [44, 45] or to the self-absorption effect due to the locally high concentration of absorbing species [20, 46]. Further pitfalls to consider in the data collection are i) the beam stability, that can lead to artefacts in the XAS data in the case of a beam motion over a

non-homogeneous area, and ii) the radiation damage that can be important considering the high photon density achieved in these beamlines ($\cong 10^{10}$ ph/s on a spot of a few μm^2).

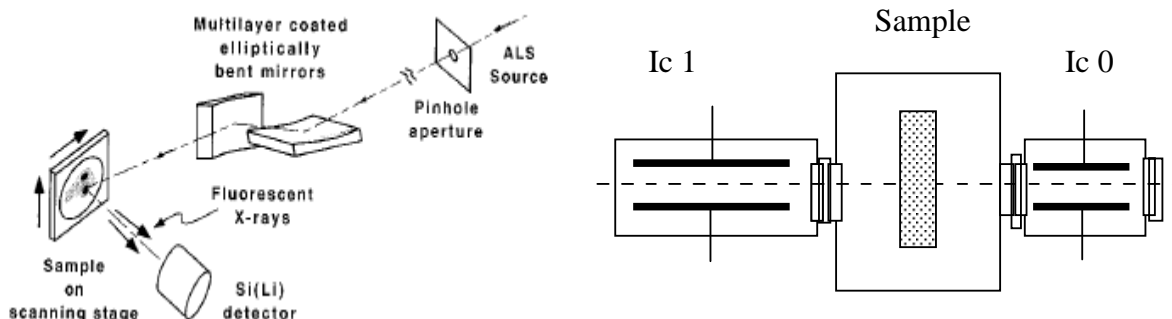


Fig. 7. Experimental setup for the measurement of the X-ray absorption coefficient of a sample.

Right: setup for transmission mode.

Left: Setup for fluorescence mode with the focussing elements and sample scanning stages (Left picture from [35]).

Note the peculiar mounting of the reflective elements (in this case 2 multilayer-coated mirrors with orthogonal reflection planes) that realize the KB assembly.

Comparison with other microscopy techniques

Hard X-ray spectro-microscopy represents a valuable tool in the analysis of intrinsically inhomogeneous samples like those encountered in environmental science, biology, cultural heritage. It offers at the same time elemental selectivity and the possibility of determining in a same experimental session both the element content (with the possibility of realising a mapping of the sample), valence state and local environment and a sensitivity of about 50 - 100 ng/g [31]. Note that XAS permits to determine local structures also in amorphous systems so there is no need of crystalline phases with long range ordering like in the case of electron diffraction techniques. In respect to electrons X-rays are by far more penetrating: the micron range can be easily achieved compared with hundreds of Å at most for the former probe: this permits the analysis of the internal part of samples that is impossible with electrons. Moreover, investigations can be carried out on insulating materials and at ambient conditions (so avoiding ultra-high vacuum environments), particularly interesting in the analysis of samples needing a controlled hydration level (namely bacteria, see [47]). With respect to techniques such as transmission electron microscopy, X-rays have the disadvantage of a lesser lateral resolution: indeed TEM can easily work in the range of the 0.2 - 20 nm [31] whereas at present X-ray beams are focussed in the 10 - 0.1 μm range [35, 36]. Moreover the availability of laboratories capable to carry out μ -XAS experiments at the best conditions is still extremely limited with

respect to the wide offer of excellent quality TEM instruments. A comprehensive review on the future trends of different microanalytical techniques is presented in [48].

EXPERIMENTAL EXAMPLES

Here some examples of application of μ -XAS and SXRF in different scientific areas are presented.

Environmental sciences

An interesting study has been published by Isaure et al. [49] on the distribution and speciation of Cd in *Arabidopsis thaliana* plant specimens. Plants were exposed to Cd salts and then the leaves and the roots were investigated by μ -SXRF and μ -XANES at the Cd-L_{III} edge. Investigations were carried out at the ESRF on the ID21 beamline [39]. SXRF has evidenced the accumulation of Cd in two peculiar regions: the trichomes (epidermal hairs) of the leaves and the central vascular part of the roots (Fig. 8).

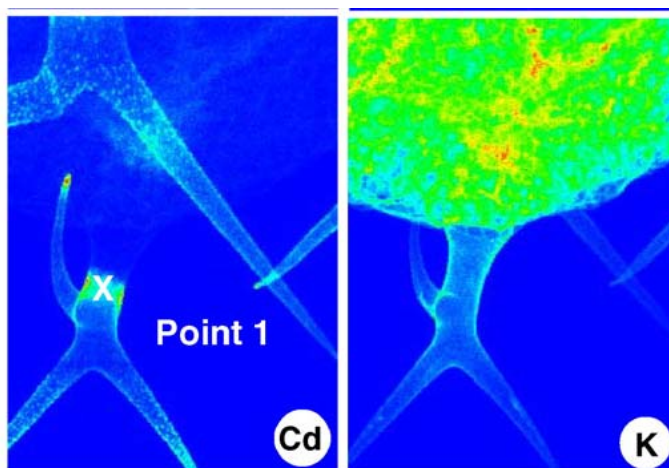


Fig. 8. SXRF image of a detail of an *Arabidopsis thaliana* leaf collected at the cadmium L α emission (left) and potassium K α emission. Potassium is present all over the leaf whereas cadmium is visible only in the surfacial trichome. The image dimensions are approx. 190*267 μm^2 . Pictures from [49].

However by carrying out a XANES analysis it has been possible to add more experimental insight on this subject, in particular to determine the local environment of Cd in the two cases. Indeed the spectra taken on the trichome and on the root differ for the features appearing in the rising part of the edge (Fig. 9): a clearly evident peak at 3,540 eV in the former case and a shoulder in the latter case. This is due to different ligands to Cd as deduced from the comparison with a number of model compounds. Compounds like Cd-pectine or

Cd-cellulose (O or N coordinated) exhibit the peak whereas those with Cd coordinated by sulphur (Cd-cysteine or Cd-glutathione) exhibit the shoulder.

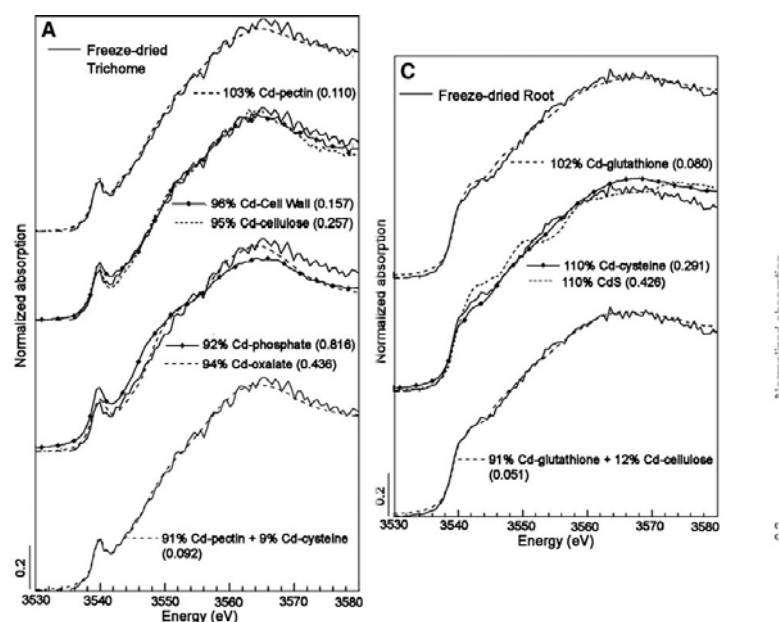


Fig. 9. μ -XANES spectra at the Cd-LIII edge on the leaf trichome (A) and on the roots (C). The spectra are markedly different (note the peak at 3,540 eV in A that reduces to a shoulder in C suggesting different types of ligands for Cd in the two cases. Pictures from [49]. The experimental spectra are then reproduced as linear combination of model compounds as shown in the captions.

By reproducing the XANES part by a linear combination of spectra of model compounds it was possible to find that in the trichomes Cd is bound to O or N whereas in the roots Cd is in a S-coordinated environment.

Biology

The following study shows a SXRF / XAS study on single bacteria of the type *Pseudomonas Fluorescens* (NCIMB 11764) [47]. The experiments were carried out at the APS synchrotron using an X-ray spot of 150 nm. The study was devoted to ascertain the feasibility of determining the elemental mapping of single bacteria in living (i.e. hydrated) conditions and to determine the valence state of a poisoning metal (Cr in this case) after interaction with the bacteria. Cells deposited on a substrate were exposed to a solution containing 1,000 ppm of Cr(VI), a strong poisoning agent, for 6 hours. After exposure the bacteria were studied by SXRF in order to establish concentration maps for the main components of living cells. Subsequently a μ -XAS investigation was carried out on the Cr in the bacteria in order to establish its redox state (Fig. 10).

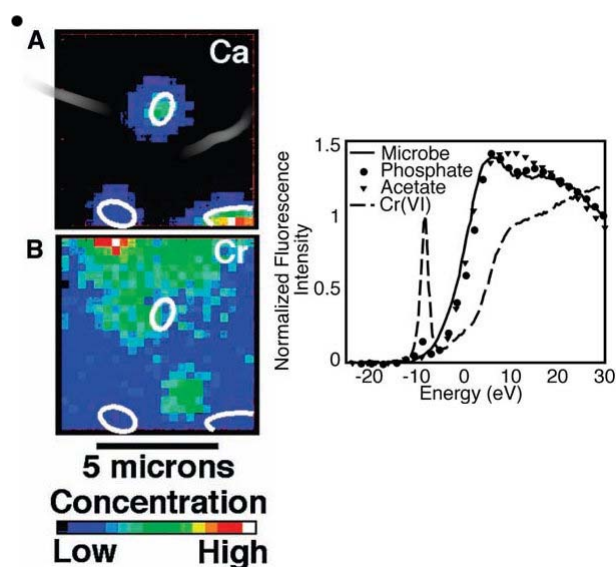


Fig. 10. Left: elemental maps for Ca (A) and Cr (B) on the *Pseudomonas Fluorescens* bacteria deposited on a substrate and exposed to Cr(VI). The colour map on the upper left side (A) shows the Ca-rich areas corresponding to the single bacteria and are evidenced by the white ovals. The same zones are shown in (B) on the Cr map. The XAS investigation has been carried out on a single bacterium containing Cr and the result is shown in the picture on the right side. Here the microbe's Cr spectrum is similar to that of Cr phosphate -Cr(III)- and markedly different from the Cr(VI) compound used to expose the cells (dash line). (Pictures from [47]).

In the right part of Fig. 10 a marked difference is evident between the spectra in the bacterium and in the original solution. Note in particular the absence of the strong absorption line 10 eV below the edge, the position of the edge itself that is placed at lower energies with respect to the Cr(VI) spectrum and the similarity with the spectrum of Cr(III) phosphate. This evidences that the bacterium has reduced Cr to a non-toxic form binding it to a phosphoryl group.

Recently an even more spatially resolved study on single cells (neurons in this case) has been published [30] with an X-ray beam of 90 nm. In this investigation it has been possible to evidence the co-localisation of Fe (revealed by SXRF) and dopamine (revealed by conventional fluorescence microscopy) in small (200 nm) vesicles inside the cells.

Cultural heritage

Also studies on cultural heritage can profit from the opportunities presented by μ -XAS. Here a study is presented devoted to find the origin of blackening of cinnabar (HgS) based pigments from a Pompeii villa [50]. The experiment was carried out at the ESRF on the ID21 beamline [39] and spectra at the sulphur K edge were collected on different samples. Here a part of the study is presented where the conventional elemental mapping is coupled to the XAS' ability to distinguish different valence states of S providing valence-sensitive

concentration maps. This is thanks to the fact that the sulphate / sulphide species exhibit maxima in emission at different energies as presented in Fig. 11.

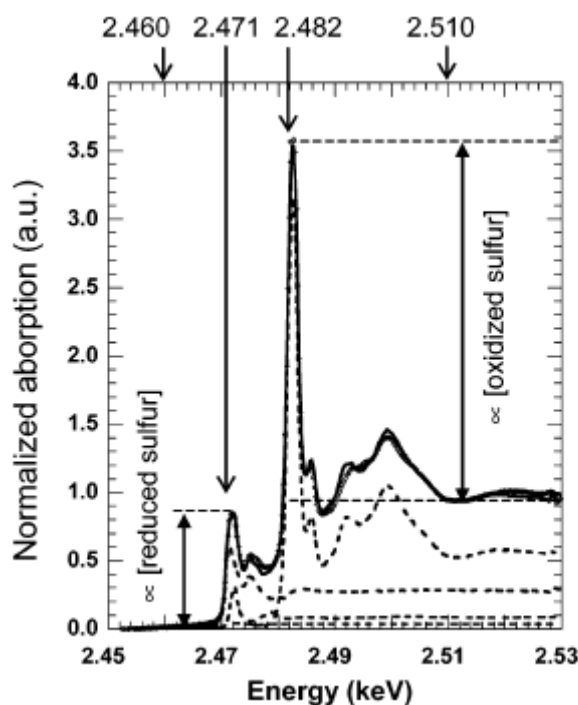


Fig. 11. μ -XANES spectra at the sulphur K-edge: fit of the experimental data (plain) on a single point by combination of cinnabar (S^{2-}), sulphur (S^0), corderoite (S^{2-}), and gypsum (S^{6+}) spectra (dotted). The picture shows also how the estimation of the reduced and oxidized sulphur concentrations are carried out by measuring the fluorescence intensity at the four specific energies indicated (from [50]).

By taking images at these energies and suitably normalising the images it has been possible to obtain maps not simply of the S content but on the reduced/oxidized sulphur species (Fig. 12).

From the analysis, it has been proposed that in the present case the blackening is not due, as previously proposed, to the structural change of the cinnabar chromophore from hexagonal to cubic because in such a case no correlation between the blackened zone and the S valence would have been observed. Rather, it is due to the extraction of S from cinnabar and the onset of the degrading process known as ‘calcite sulphation’.

An analogous space-resolved study with valence-state mapping has been published on copper-containing weathered church glasses by Farges et al. [51] carried out at the bending magnet beamline 10.3.2 [52] at the Advanced Light Source.

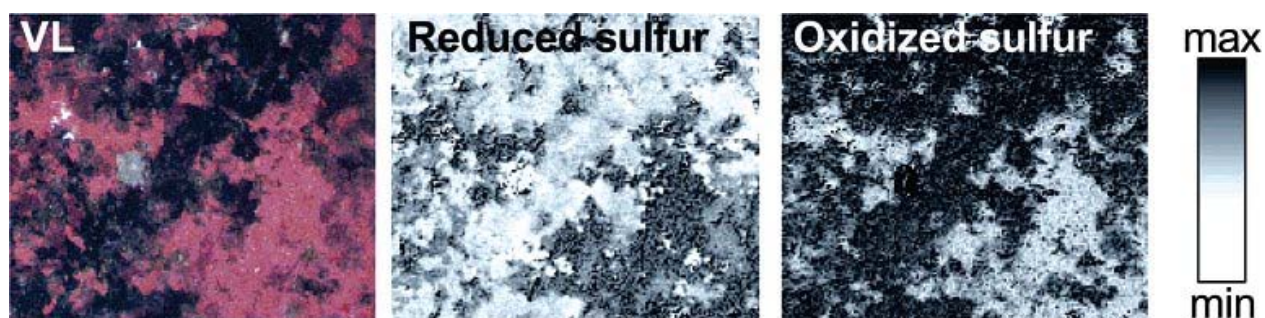


Fig. 12. Comparison between the visible light image of a blackened pigment specimen (note the central black stripe) and the images obtained from the analysis of the S K α fluorescence line intensity from reduced sulphur (maximum intensity at 2,471 eV) and oxidized sulphur (maximum intensity at 2,482 eV). The blackened region corresponds to an enriched zone of oxidized sulphur corresponding to a depleted zone of the reduced species. The analyzed regions have a dimension of 8*7 mm² and were sampled with pixels of 50*50 μ m. Picture from [50].

PERSPECTIVES

The future of μ -XAS / μ -SXRF facilities will depend on the availability of beamlines with suitably sized beams and on the development of fast techniques for sampling. The latter issue is particularly critical for XAS maps where the collection of several thousands points is impossible with the present methods whereas 500*500 points maps are routinely collected in the case of SXRF data. On the side of the facilities the European Synchrotron Radiation Source is currently preparing a scientific programme for the 2008-2017 decade where the availability of focal spots of nanometre size is one of the main issues. The goal will be to make routinely available, on a number of dedicated beamlines, focal spots of the order of 50 nm by realising optical systems with a limited number of components and an extremely high (\cong 1000) demagnification [53]. In practice this will be realized by using long (150 m) beamlines with a single KB device with a focal length of about 10 cm.

On the side of the data collection there is the proposal to collect XAS data in energy-dispersive mode [54] in order to minimize the collection time [55]. Following this original idea, the collection time of an hypothetical XAS map in a 1*1 mm² region at 1 μ m steps (106 spectra) could drop from 11 days with a standard stepping monochromator (even at the noticeably short collection time of 1s/spectrum) to a few hours with a collection time of 10 ms typical for the energy-dispersive XAS apparatus. A beamline using energy-dispersive XAS and dedicated to this kind of studies will be realized during the upgrade programme of the ESRF [53].

Eventually, we point out some pioneering research activity on a novel experimental technique consisting in using a scanning probe microscope to detect signals from a sample illuminated with synchrotron radiation. In this case, the spatial resolution is determined by the

microscope tip dimensions and not by the X-ray beam size thus permitting data collection on single nanostructures like quantum dots or similar. Lateral resolution in the nm range is easily achieved even with much larger focal spots. This provides a technique less prone to spurious signals coming from occasional movements of the beam. Preliminary results have been published, using the microscope in electrostatic force mode [56] or in total electron yield mode [57] that, although still remaining at an extremely qualitative stage, represent an interesting possible evolution in the field of μ -XAS.

REFERENCES

- [1] F. d'Acapito, S. Colonna, S. Pascarelli, G. Antonioli, A. Balerna, A. Bazzini, F. Boscherini, F. Campolungo, G. Chini, G. Dalba, I. Davoli, P. Fornasini, R. Graziola, G. Licheri, C. Meneghini, F. Rocca, L. Sangiorgio, V. Sciarra, V. Tullio and S. Mobilio (1998) *ESRF Newsletter*, **30**, 42.
see also <http://www.esrf.fr/UsersAndScience/Experiments/CRG/BM08/>.
- [2] D.E. Sayers, E.A. Stern and F.W. Lytle (1971) *Phys. Rev. Lett.*, **27**, 1204.
- [3] B.M. Kincaid and P. Eisenberger (1975) *Phys. Rev. Lett.*, **34**, 1361.
- [4] P.A. Lee, P.A. Citrin, P.H. Eisenberger and B.M. Kincaid (1981) *Rev. Mod. Phys.*, **53**, 769.
- [5] D.C. Königsberger (1988) *X-ray absorption* (D.C.Königsberger and R.Prins, Eds.). John Wiley and Sons, New York.
- [6] J.J. Rehr and R.C. Albers (2000) *Rev. Mod. Phys.*, **72**, 621-654.
- [7] E.A. Stern (1988) in *X-ray absorption* (D.C.Königsberger and R. Prins, Eds.). John Wiley and Sons, New York.
- [8] G. Beni and P.M. Platzmann (1976) *Phys.Rev. B*, **14**, 1514.
- [9] E. Sevillano, H. Meuth and J.J. Rehr (1979) *Phys.Rev. B*, **20**, 4908.
- [10] A.V. Poiarkova and J.J. Rehr (1999) *Phys. Rev. B*, **59**, 948.
- [11] Chou (1987).
- [12] P.A. Lee and G. Beni (1977) *Phys.Rev. B*, **15**, 2862.
- [13] E.A. Stern (1971).
- [14] A. Filipponi, A. DiCicco and C.R. Natoli (1995) *Phys.Rev B*, **52**, 15122-15134.
- [15] A. Filipponi and A. DiCicco (1995) *Phys.Rev. B*, **52**, 15135-15149.
- [16] S.I. Zabinsky, J.J. Rehr, A. Ankudinov, R.C. Albers and M.J. Eller (1995) *Phys. Rev. B*, **52**, 2995-3009.
- [17] B. Ravel and M. Newville (2005) *J. Synchrotron Rad.*, **12**, 537-541.
- [18] N. Binsted (1998) EXCURV98. CCLRC Daresbury Laboratory computer programme; see also <http://srs.dl.ac.uk/XRS/index.html>
- [19] A. Manceau, B. Lanson, M.L.L. Schlegel, J.C. Hargé, M.E. Musso, L. Eybert-Berard, J.-L. Hazemann, D. Chateigner and G.M. Lamble (2000) *Amer. J. Science*, **300**, 289-343.
- [20] A. Manceau, M.A. Marcus and N. Tamura (2002) *Rev. Mineral. Geochem. Miner. Soc. America*, **49**, 341-428.

- [21] M.J. Fay, A. Proctor, D.P. Hoffmann, M. Houalla and D.M. Hercules (1992) *Mikrochim Acta*, **109**, 281-293.
- [22] S.R. Wasserman, R.E. Winans and R. McBeth (1996) *Energy & Fuels*, **10**, 392-400.
- [23] T. Ressler, J. Wong, J. Roos and I.L. Smith (2000) *Environ Sci. Technol.*, **34**, 950-958.
- [24] C.R. Natoli and M. Benfatto (1986) *J. de Phys Coll.*, **C8**, 11.
- [25] M. Benfatto C.R. Natoli, A. Bianconi, J. Garcia, A. Marcelli, M. Fanfoni and I. Davoli (1986) *Phys. Rev. B*, **34**, 5774.
- [26] M. Benfatto and S. Della Longa (2001) *J. Synchrotron Rad.*, **8**, 1087-1094.
- [27] S. Della Longa, A. Arcovito, M. Girasole, J.L. Hazemann and M. Benfatto (2001) *Phys. Rev. Lett.*, **87**, 155501.
- [28] F. Studer D. Bourgault, C. Martin, R. Retoux, C.B. Raveau, E. Dartyge and A. Fontaine (1989) *Physica C*, **159**, 609-615.
- [29] L. Galois, G. Calas and M.A. Arrio (2001) *Chem. Geol.*, **174**, 307-319.
- [30] R. Ortega, P. Cloetens, G. Deves, A. Carmona and S. Bohic (2007) *PloS ONE*, **2**, e925.
- [31] P.M. Bertsch and D.B. Hunter (2001) *Chem. Rev.*, **101**, 1809-1842.
- [32] B. Lai, W.B. Yun, D. Legnini, Y. Xiao, J. Crzas, P.J. Viccaro, V. White, D. Denton, F. Cerrina, E. Di Fabrizio, L. Grella and M. Baciocchi (1992) *Appl. Phys. Lett.*, **61**, 1877-1879.
- [33] B. Lengeler, C.G. Schroer, M. Richwin, J. Tümmeler, M. Drakopoulos, A. Snigirev and I. Snigireva (1999) *Appl. Phys. Lett.*, **74**, 3924-3926.
- [34] D.J. Thiel, D.H. Bilderback and A. Lewis (1993) *Rev. Sci. Instrum.*, **64**, 2872-2878.
- [35] P. Dhez, P. Chevallier, T.B. Lucatorto and C. Tarrío (1999) *Rev. Sci. Instrum.*, **70**, 1907-1920.
- [36] O. Hignette, P. Cloetens, G. Rostaing, P. Bernard and C. Morawe (2005) *Rev. Sci. Instrum.*, **76**, 063709.
- [37] A.-M. Flank, G. Cauchon, P. Lagarde, S. Bac, M. Janousch, R. Wetter, J.-M. Dubuisson, M. Idir, F. Langlois, T. Moreno and D. Vantelon (2006) *Nucl. Instrum. and Meth. B*, **246**, 269-274.
- [38] A. Somogy, T. Tucoulou, G. Martinez-Criado, A. Homs, J. Cauzid, P. Bleuet, S. Bohic and A. Simionovici (2005) *J. Synchrotron Rad.*, **12**, 208-215.
- [39] J. Susini, M. Salome, B. Fayard, R. Ortega and B. Kaulich (2002) *Surf. Rev. Lett.*, **9**, 203-211.
- [40] See web site <http://www.anl.gov/> for updated information.
- [41] S. Hayakawa, N. Ikuta, M. Suzuki, M. Wakatsuki and T. Hirokawa (2001) *J. Synchrotron Rad.*, **8**, 328-330.
- [42] M. Awaji, Y. Suzuki, A. Takeuchi, H. Takano, N. Kamijo, S. Tamura and M. Yasumoto (2001) *Nucl. Instrum. Methods A*, **467/468**, 845-848.
- [43] J. Jaklevich, J.A. Kirby, M.P. Klein, A.S. Robertson, G.S. Brown and P. Eisenberger (1977) *Sol. St. Comm.*, **23**, 679.
- [44] G.F. Knoll (2000) *Radiation Detection and Measurement, 3rd Edition*. John Wiley & Sons, New York.

- [45] G. Ciatto, F. d'Acapito, F. Boscherini and S. Mobilio (2004) *J. Synchrotron Rad.*, **11**, 278-283.
- [46] P. Pfalzer, J.-P. Urbach, M. Klemm, S. Horn, M.L. Den Boer, A.I. Frenkel and J.P. Kirkland (1999) *Phys. Rev. B*, **60**, 9335.
- [47] K.M. Kemner, S.D. Kelly, B. Lai, J. Maser, E.J. O'Loughlin, D. Sholto-Douglas, Z. Cai, M.A. Schneegurt, C.F. Kulpa, Jr. and K.H. Nealson (2004) *Science*, **306**, 686-687.
- [48] F. Adams, L. Van Vaeck and R. Barrett (2005) *Spectrochimica Acta B*, **60**, 13-26.
- [49] M.P. Isaure, B. Fayard, G. Sarret, S. Pairis and J. Bourguignon (2006) *Spectrochim. Acta B*, **61**, 1242-1252.
- [50] M. Cotte, J. Susini, N. Metrich, A. Moscato, C. Gratziu, A. Bertagnini and M. Pagano (2006) *Anal. Chem.*, **78**, 7484-7492.
- [51] F. Farges., M.-P. Etcheverry., A. Scheidegger and D. Grolimund (2006) *Appl. Geochem.*, **21**, 1715-1731.
- [52] M.A. Marcus, A.A. MacDowell, R. Celestre, A. Manceau, T. Miller, H.A. Padmore and R.E. Sublett (2004) *J. Synchrotron Rad.*, **11**, 239-247.
- [53] European Synchrotron Radiation Facility, *Science and technology programme 2008-2017*; available at <http://www.esrf.fr>
- [54] T. Matsushita and R.P. Phizackerley (1981) *Jpn. J. Appl. Phys.*, **20**, 2223-2228.
- [55] S. Pascarelli, O. Mathon., M. Munoz, T. Mairs and J. Susini (2006) *J. Synchrotron Rad.*, **13**, 351-358.
- [56] M. Ishii, B. Hamilton, N. R. J. Poolton, N. Rigopoulos, S. De Gendt and K. Sakurai (2007) *Appl. Phys. Lett.*, **90**, 063101.
- [57] P. Dhez, M. Rodrigues, F. Comin, R. Felici and J. Chevrier (2007) *AIP Conf. Proc.*, **879**, 1391-1394.